Cellulose (2019) 26:1769–1780
https://doi.org/10.1007/s10570-018-2164-x

ORIGINAL RESEARCH

Fabrication and characterization of emulsified and freeze-dried epoxy/cellulose nanofibril nanocomposite foam

Jinghao Li · Qiangu Yan · Zhiyong Cai

Received: 17 July 2018 / Accepted: 27 November 2018 / Published online: 18 December 2018

Abstract Utilization of cellulose nanofibril (CNF) material for light weight and high strength structural composites has attracted considerable attention in the recent years. CNF aerogels have a microporous structure that could have potential properties, such as ultra-low density, high porosity, high specific surface area, high flexibility, and low thermal conductivity. However, producing such a product is still somewhat problematic. In this study, an epoxy/CNF (EP/CNF) nanocomposite foam with micro-rib structures has been developed using emulsification combined with freeze-dried processes. The microstructures of these new EP/CNF composite foams were observed using a scanning electron microscope. The surface morphology showed that CNF fiber walls were uniformly sealed with epoxy resin after curing. Mechanical properties, water resistance, and thermal stability of the EP/CNF composites foams were tested using the compression test, water absorption test, and thermogravimetric analysis. The results showed that the CNFs played an important role in forming a skeleton like structure within these composite foams. The amount of EP in the EP/CNF emulsions had significant effect on the compressive properties and water resistance. Samples fabricated with higher epoxy content had higher compressive properties, better water resistance, and thermal stability. The epoxy/CNF nanocomposites properties were significantly improved as compared to pure CNF aerogel. The glass transition temperature (T_g) of the nanocomposites was influenced by the EP/CNF composition. The mechanical and physical properties of EP/CNF nanocomposite foams could be optimized via changing the weight ratio of epoxy resin in EP/CNF emulsion according to the demanding of specific application.

J. Li · Q. Yan · Z. Cai (✉)
USDA Forest Service, Forest Products Laboratory,
Madison, WI 53726, USA
e-mail: zcai@fs.fed.us

Graphical abstract

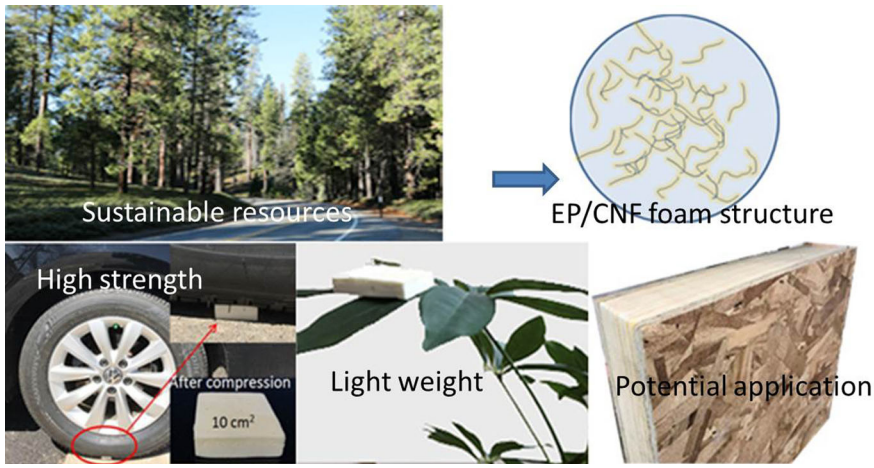

Keywords Emulsification · Cellulose · Epoxy · Characteristic · Foam · Properties

Introduction

In the past two decades, significant attention has been devoted toward the development and investigation of polymer nanocomposites where high-efficiency microstructure and nanoscale filler provided excellent mechanical properties for a variety of engineering applications such as building materials, packaging, automotive and transportation (Fowler et al. 2006; Leng et al. 2017). Cellulose, with production levels around 1.5×10^{12} tons each year, is one of the most abundant biopolymers on earth. Cellulose is a biodegradable and renewable resource that attracts particular interest as a raw material (Zhang et al. 2016). Cellulose nanofibrils (CNFs), a nano component of cellulose has shown remarkable mechanical properties (Lee et al. 2009). Recently, the utilization of CNFs for light weight nanocomposites has attracted attention (Khalil et al. 2012). When CNF size was reduced from bulk wood cells to nanofibrils, their elastic modulus increased, ranging from 10 to 70 GPa (Jeronimidis 1979), which provides great potential for developing new eco-friendly nanocomposite materials having high strength to weight characteristics for some engineering applications (Bledzki and Gassan 1999).

The high surface area CNFs with many chemical function groups makes it a good candidate for the production of aerogel. CNF with self-assembled or self-bonding characteristics is an attractive biopolymer nanomaterial for production of multi-functional aerogels due to its biodegradability, biocompatibility, availability, renewability, and load capacity. The skeletal-like structure of CNF aerogel can be formed without collapsing by the removal of liquid, which can produce an ultra-lightweight material. To obtain this light-weight structure, the gel material is dried using supercritical carbon dioxide drying, freeze-casting, and vacuum-drying in which CNF aerogels can be functionalized for different applications such as superabsorbent, supercapacitor, and photoanode materials (Chen et al. 2016; Li et al. 2014b; Zheng et al. 2014, 2015). Because the ultra-micro-porous structure of CNF aerogel provides lightweight characteristics, it presents an opportunity to develop eco-friendly alternatives for structural composites in engineering applications (Ahmadzadeh et al. 2016; Han et al. 2017). However, the current low relative strength and high water solubility of pure CNF aerogel are still obstacles when competing with synthetic foam products.

Epoxy resin, is a structural resin with high strength, good stability and wide compatibility that is used for many engineering applications (Hodgkin et al. 1998). Epoxy resin could be an ideal co-material option for CNF nanocomposite foams. However, most epoxy resins exhibit high viscosity, making it difficult to penetrate into micro porous CNF aerogel. In the previous study (Li et al. 2018), a fabrication process was developed to produce EP/CNF nanocomposite

foams where differing strength and performance levels of the foams were obtained based on their differing formulations. These composite foams were produced by mixing epoxy in a dilute mixture of either ethyl acetate (EA) or tetrahydrofuran (THF) solvent in combination with CNFs. Those solvents added extra cost and potential toxicity when using this fabrication approach. In this study, an EP/CNF emulsion was developed to form the EP/CNF nanocomposite foam without a solvent for sandwich structural panels (Li et al. 2014a, 2017a, b). The morphology, crystalline structure, and thermal and physical properties of the new formulations of EP/CNF nanocomposite foams were measured and analyzed using a scanning electron microscope (SEM), water absorption test, thermogravimetric analysis (TGA), compression test, differential scanning calorimetry (DSC), and Fourier transform infrared spectroscopy (FTIR).

Materials and methods

Materials

TEMPO oxidized CNF suspensions used in this experiment were prepared in USDA Forest Products Laboratory (Madison, WI, US) according to the work reported by Saito et al. (2009). Commercial No. 635 epoxy resin (containing 70–90% 4,4′-isopropylidenediphenol-epichlorohydrin copolymer by weight), with a ratio of 3:1 for resin and hardener, was obtained from US Composites Inc. (West Palm Beach, FL, US) for the matrix of EP/CNF composite foam.

Experiments and preparation of EP/CNF composite foam

Figure 1 shows the fabrication processes of EP/CNF composite foam. The epoxy resin and hardener were mixed and added into 0.9 wt% TEMPO-oxidized CNF suspensions with a dry CNF weight ratio of 5%, 10%, and 15%, respectively. The resulting solutions were further mixed via mechanical mixer at a speed of 400 rpm for 5 min, prior to 10 min sonication for emulsification. After these processes, EP/CNF emulsions with different ratios were obtained and then cooled to − 78 °C for 2 h by CO_2-based freezer (The size, sharp, and quantity of porous structure of nanocomposite foam can be controlled by the pre-freezing temperature. Generally, the higher temperature forms larger porous size of foam in terms of ice crystal growth.) before freeze-drying using a Labconco freeze-drying system (Kansas City, MO, USA). The samples were held under a vacuum of 0.01 MPa at a temperature of − 105 °C for 3 days. After the freezing-dry process, the dehydrated EP/CNF aerogel samples were cured using a vacuum oven at 60 °C for 2 h. The EP/CNF nanocomposite foam was stored in a desiccator for further testing and characterizations. The pure CNF sample was fabricated using the same process as well as EP/CNF composite foam except epoxy resin. The neat epoxy sample was made by mixing and curing No. 635 epoxy resin at room temperature, because the porous structural neat epoxy cannot be formed using the same emulsified and freeze-dried method without CNF component. The controls and mixtures of EP/CNF composite foams are shown in Table 1.

Morphology

CNF aerogel, neat epoxy resin, and EP/CNF composite samples were cryosectioned to visualize both the internal and external surface morphologies. The sectioned samples were mounted with conductive carbon tape, sputter coated with gold and imaged using field emission scanning electron microscope (FE-SEM) at a 5 mm working distance and a 5 kV accelerating voltage.

Compression test

Compression tests were performed on EP/CNF composite foams following ASTM D695-15 (2010). The samples measured 12.5 mm × 12.5 mm × 6.4 mm and were conditioned at 23 °C and 65% relative humidity for 2 weeks prior to testing. Five replicates were tested for each formulation. Their density, compressive strength, and elastic modulus were reported in the study. All specific properties were calculated by normalizing the measured strength and modulus with the measured density (ρ, kg/m^3) of each sample type.

Water absorption test

The conditioned samples were precisely weighed and then immersed in distilled water. Samples were

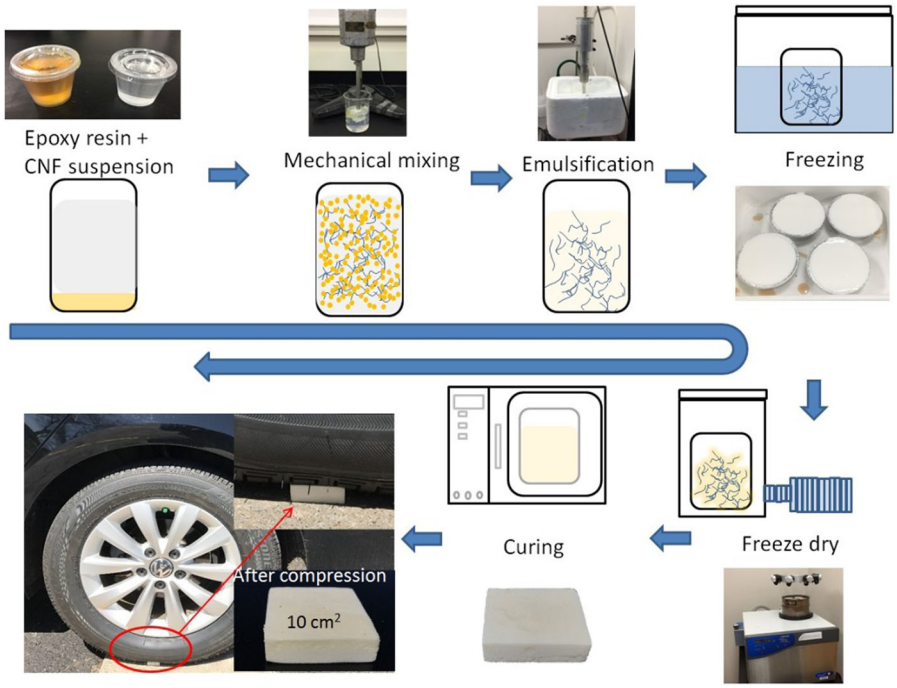

Fig. 1 Schematic illustration of the fabrication process of EP/CNF nanocomposite foam

Table 1 The compositions of EP/CNF composite foam

Sample	CNF weight content ratio in the foam (%)	Epoxy weight content ratio in the foam (%)
CNF	100	0
Epoxy	0	100
EP/CNF15	15	85
EP/CNF10	10	90
EP/CNF5	5	95

removed after 20 min and left to stand on a culture dish for 2 min before weighing. This process was performed at approximately 20 min intervals until the data trend stabilized, and then the measurement was performed at 4 h increments over a span of 24 h. After that, the subsequent measurements were performed at 24 h intervals over a span of 288 h until reaching equilibrium. Five replicates in each group were tested. Water absorption was calculated using the equation according to (ASTM D570-98 1998):

$$\text{Water absorption } (\%) = \frac{W_t - W_0}{W_0} \times 100\% \quad (1)$$

where W_t and W_0 denote the weight of sample after and before water absorption test, respectively.

Thickness swell was calculated by the equation based on (Kord 2013):

$$\text{Thickness swelling } (\%) = \frac{T_t - T_0}{T_0} \times 100\% \quad (2)$$

where T_0 is initial sample thickness and T_t is thickness at time t.

Moisture diffusion coefficients (D_f) of EP/CNF samples were calculated using Eq. (2) (Wei et al. 2013):

$$D_f = \pi(h/(4M_\infty))^2 \left(\Delta M/\Delta t^{\frac{1}{2}}\right)^2 \quad (3)$$

where M_∞ is the maximum moisture content measured at the end of the test, h is the sample thickness corresponding to M_∞, t is time, and $\Delta M/\Delta t^{\frac{1}{2}}$ is the initial slope from the MC versus $t^{1/2}$ relation.

Thermal stability (TGA)

Thermal stability of neat CNFs, epoxy, and nanocomposites were assessed by TGA (PerkinElmer Thermogravimetric Analyzer, Pyris 1 TGA). Samples (1–3 mg) were heated from 50 to 650 °C with a rate of 10 °C/min under a flow rate of 20 mL/min nitrogen at atmospheric conditions.

Wide angle X-ray diffraction (XRD) measurement

X-ray diffraction (XRD) patterns were obtained with a Bruker Discovery 8 diffractometer using Cu Kα rotation tube at 50 kV and 1000 μA with scanning over the range of 2θ = 5°–50°.

Thermal analysis (DSC)

Differential scanning calorimetry (DSC) was performed on neat epoxy and nanocomposite samples (5 mg) using a TA instrument model Q200 DSC with refrigerated cooling. The samples were (i) equilibrated at − 50 °C (3 min) then ramped to 160 °C at 10 °C/min. Data were analyzed using TA Universal Analysis v4.5A software. The glass transition temperature (T_g) was determined from the heating scan curve.

Fourier transform infrared Spectroscopy (FTIR)

The FTIR spectra of pure CNFs, neat epoxy and EP/CNF composite samples were recorded with the Thermo Scientific ATR-FTIR spectrometer (Thermo Scientific, Nicolet iZ10) at a resolution of 4 cm^{-1} for 64 scans in 500–4000 cm^{-1} range. All powdered samples were pressed against the diamond crystal of the ATR device. Background spectrum obtained by scanning the air was subtracted from the sample spectrum before converted into transmittance units.

Results and discussion

Morphology

Figure 2 shows the morphologies of pure CNF aerogel and cured neat epoxy resin. The flake-like (or sheet-like) CNF walls were observed in the pure CNF aerogel sample (Fig. 2a). When comparing CNF aerogel with the neat epoxy resin, small resin particles were uniformly distributed in Fig. 2b after resin curing at room temperature. Figure 3 shows EP/CNF nanocomposite foam samples with different weight ratios. The flake-like layered microstructure was observed on the EP/CNF nanocomposites fabricated with EP/CNF emulsion. After emulsification process, the CNF aerogels were encapsulated with epoxy resin as shown in Fig. 3a. As epoxy weight ratios increased in the samples, epoxy micro-ribs were observed on the EP/CNF flake-like walls as shown in Fig. 3b. By further increased amounts of epoxy, EP/CNF5 samples, there were more epoxy micro-ribs and cross-linked structure that occurred on the CNF wall (Fig. 3c). The micro-ribs connected each CNF wall which provided a larger apparent lateral section to resist external loads. In the experiments, we also found that the porous size can be controlled by the pre-freezing temperature. The microstructure of aerogel was determined by the size and growth direction of ice crystal in the pre-freezing process.

Mechanical properties

Compression tests were performed on the EP/CNF nanocomposite foams to determine compressive modulus, strength, and specific compressive properties. The density, compressive modulus, and compressive strength of CNF aerogel and EP/CNF composite foams are shown in Table 2. CNF aerogel displayed an ultra-light weight density of 13.0 kg/m^3. However, it had very low compressive modulus and compressive strength, which was only 0.083 MPa and 0.011 MPa, respectively. With the addition of epoxy resin into the CNF suspension, the epoxy resided in the CNF structure after freeze-drying and curing. The densities increased with increasing epoxy content. The density of EP/CNF5 with 95% epoxy weight ratio was 149.7 kg/m^3, which was significantly greater than the other samples with lower epoxy content. In

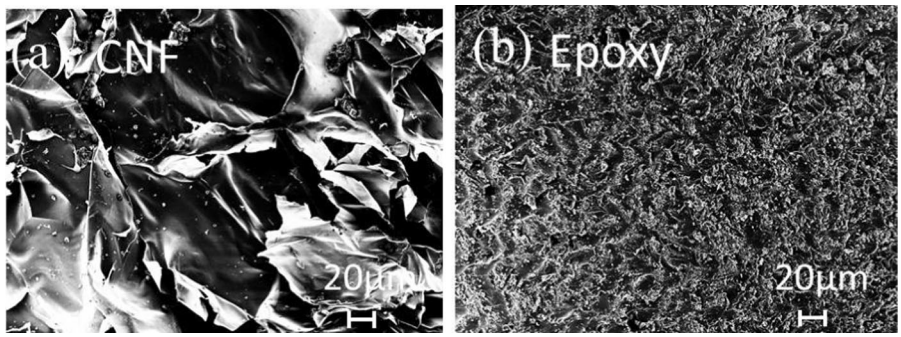

Fig. 2 SEM micrographs of CNFs and epoxy: **a** CNFs; **b** epoxy

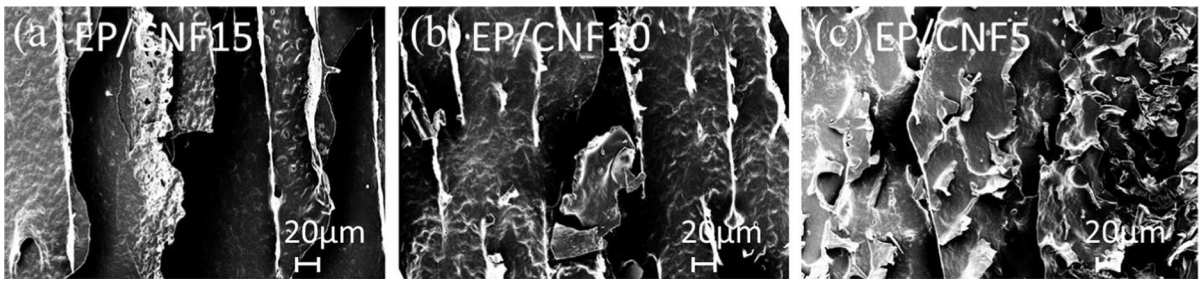

Fig. 3 SEM micrographs of EP/CNF nanocomposite foam: **a** EP/CNF15; **b** EP/CNF10; **c** EP/CNF5

Table 2 Density, compressive modulus, and compressive strength of samples (mean ± SE) with different epoxy concentrations

Sample	Density ρ (kg/m^3)	Compressive modulus E (MPa)	Compressive stress σ (MPa)
CNF	13.0 ± 0.7^a	0.083 ± 0.027^a	0.011 ± 0.0003^a
EP/CNF15	65.4 ± 0.7^b	2.25 ± 0.44^{ab}	0.17 ± 0.016^{ab}
EP/CNF10	83.5 ± 0.7^c	8.51 ± 0.79^c	0.46 ± 0.030^{bc}
EP/CNF5	149.7 ± 1.2^d	23.88 ± 0.79^d	1.67 ± 0.19^d

The properties, samples with same letter are not significantly different at the 95% confidence interval of probability using Tukey tests

comparison, the pure or solid density of the epoxy was 1101 kg/m^3.

The compressive modulus and compressive strength values increased with the increasing epoxy content. Noticeably, compressive modulus and strength values for EP/CNF5 were 23.88 MPa and 1.67 MPa, respectively, as compared to the CNF aerogel only values of 0.083 MPa and 0.001 MPa, respectively. The EP/CNF compressive moduli were 26 and 102 times greater than pure CNF foam for 15% and 10% CNF addition, respectively. The EP/CNF compressive strengths were 14 and 41 times greater than pure CNF foam for 15% and 10% CNF addition, respectively. These values were due to greater levels of epoxy resin uniformly compounded into the CNFs skeleton-like structures, and crosslinked ribs between the CNFs structural walls which limited transverse deformation and buckling while resisting compressive loads. The resin crosslinked ribs structure was indicated from the morphological studies in Fig. 3c.

The changes in density ρ, with the addition of epoxy, were statistically significant at $P < 0.05$ (Table 2). By normalizing compressive properties as a function of density, values can be compared to other CNF based composites. The plots of specific compressive properties are shown in Fig. 4a, b. The pure CNF aerogel shows very low E/ρ (0.006 MPa) and σ/ρ (0.008 MPa) as compared with the EP/CNF foam. As

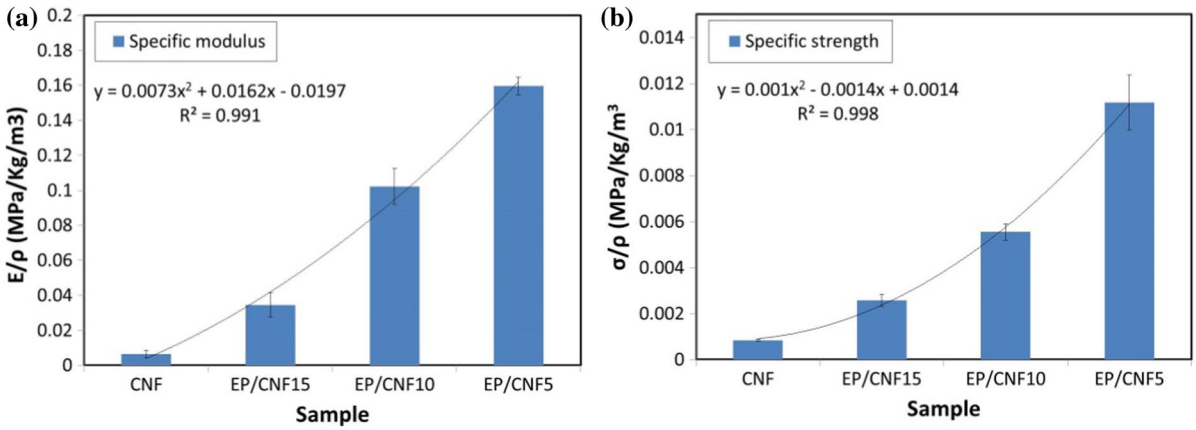

Fig. 4 **a** Specific compressive modulus of EP/CNF composite foams; **b** specific compressive strength of EP/CNF composite foams with decreasing percentages of CNF

epoxy loading increased from 85 to 95%, both the E/ρ and σ/ρ of EP/CNF foams increased. Notably, the E/ρ and σ/ρ of EP/CNF5 increased by 362% and 332% when the ratio of resin of EP/CNF nanocomposites was increased from 85 to 95%, respectively. Regression models were made for both E/ρ and σ/ρ. Both quadratic regression models for E/ρ and σ/ρ had good agreement with experimental results, which had a very high correlation coefficient R^2 at 0.991 and 0.998, respectively. Epoxy significantly reinforced the mechanical performance of pure CNF aerogel with the emulsified EP/CNF, meanwhile, a center amount of CNFs is essential component to make the structure support for this EP/CNF nanocomposite foam. The mechanical and physical properties of EP/CNF nanocomposite foam can be controlled in terms of the ratio of EP/CNF to some extent. The EP/CNF composites foam has better compression performance and specific compressive strength than that of similar cellulose aerogels reinforced by polyvinyl alcohol-borax and clay in the same density range (Ahmadzadeh et al. 2016; Han et al. 2017). Furthermore, all samples had less standard error than the EP/CNF foams made by resin infusion process, and higher structural uniformity can be achieved by the emulsion method for EP/CNF nanocomposite foam (Li et al. 2018).

Thermal properties

Thermal stability is a vital characteristic for structural materials. TGA data for pure CNFs, neat epoxy, and EP/CNF foams are shown in Fig. 5. Thermal degradation of pure CNF aerogel occurred at a temperature around 215 °C in nitrogen atmosphere, which was the same as presented in the literature (Soni and Mahmoud 2015), and the entire pyrolysis of pure CNF aerogel was from 180 to 375 °C. The amount of char residue for pure CNF aerogel was 26.3% at 600 °C. For the neat epoxy resin, the mass loss displayed only one major distinctive stage between 350 and 450 °C. Moreover, the EP/CNF foam had higher temperature at maximum weight loss rate (T_{max}) and lower char residue than pure CNF samples. As epoxy weight increased in the EP/CNF emulsion, the degradation temperature of EP/CNF nanocomposite foam samples at maximum weight loss rate also increased and all the samples with different EP/CNF formulas had slightly higher temperature at maximum weight loss rate than the neat epoxy sample. The (T_{max}) of EP/CNF15, EP/CNF10, and EP/CNF5 increased by 32.3 °C, 30.3 °C, and 29.0 °C as compared to neat epoxy sample, respectively. This could be attributed to the interlocking of CNFs and epoxy resin, which required additional energy inputs and time to degrade the nanocomposites foam. The porous structure and thermal conductivity property of the nanocomposite foam could also be factors to delay the heat transfer so that more energy was consumed for low density EP/CNF foam. The EP/CNF foam samples with higher epoxy weight content had lower char residue. Because the char residue was contributed primarily by the CNF aerogel, the char residue for CNF aerogel at 600 °C was over 4 times higher than the neat epoxy sample at

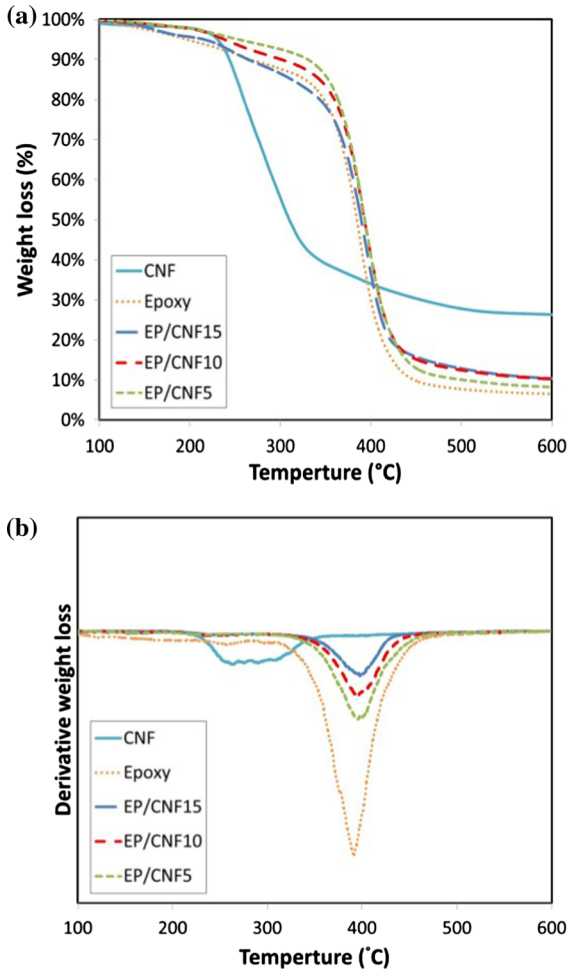

Fig. 5 TGA **a** weight loss; **b** derivative of weight loss versus temperature for pure CNFs, epoxy, and EP/CNF nanocomposites

6.4%. The char residue of EP/CNF15, EP/CNF10, and EP/CNF5 were 10.4%, 9.8% and 8.2%, respectively, which were gradually decreased as CNF weight content decreased. The epoxy had higher degradation temperature than CNFs so that significantly improved thermal stability of EP/CNF aerogel.

Glass transition temperature (T_g) for the CNFs and EP/CNF composites were measured using the DSC, as shown in Table 3. Results showed that the presence of CNFs increased the T_g compared with neat epoxy and this effect was even more pronounced for sample EP/CNF15 where the T_g temperature was 64.5 °C. The T_g for EP/CNF5 was lower than those for EP/CNF15 and EP/CNF10. This suggests that more epoxy in CNF emulsion covered the CNF microstructural wall after

Table 3 T_g of each sample with different formula determined by DSC

Sample	T_g (°C)
EPOXY	47.2
EP/CNF15	64.5
EP/CNF10	64.2
EP/CNF5	63.3

Difference between duplicates was less than 0.1%, so the standard deviation was not added

the freeze-drying and curing steps for EP/CNF foam. Although the T_g value of EP/CNF15 was slightly higher than the value of EP/CNF10, the results indicated that T_g had no significant change when epoxy was slightly lower than the saturation level. The small change of T_g for the samples with low density was attributed to the porous and discontinuous interlocking structure of EP/CNF foam, which may require more energy to soften sample when epoxy cannot completely coat the CNF foam. Moreover, the glass transition temperature of EP/CNF nanocomposite foam was dominated by epoxy resin. Other type of epoxy resin with higher glass transition temperature could be used to increase the glass transition temperature of EP/CNF nanocomposite foam.

Water absorption

After EP/CNF nanocomposites were immersed in DI water for 288 h (12 days), the absolute water absorption (WA) curves were plotted, as shown in Fig. 6a, by the percentage weight gain as a function of time. The pure CNF aerogel dissolved in DI water very quickly while the neat cured epoxy resin is a water insoluble material, thus neither sample was reported in Fig. 6. Results show the WAs increased for EP/CNF samples fabricated by emulsified EP/CNFs with decreasing epoxy loading. The EP/CNF15 sample had highest water absorption of 1230.1%, followed by samples of EP/CNF10 and EP/CNF5 at 709.5% and 335.4%, respectively. This indicated that the higher the epoxy loading in the sample can somewhat encapsulate the surfaces of hydrophilic CNFs, and block water absorbing into the porous structures via crosslinking, whereby water cannot contact soluble CNF portions of the epoxy interior. Thus, low water absorption was

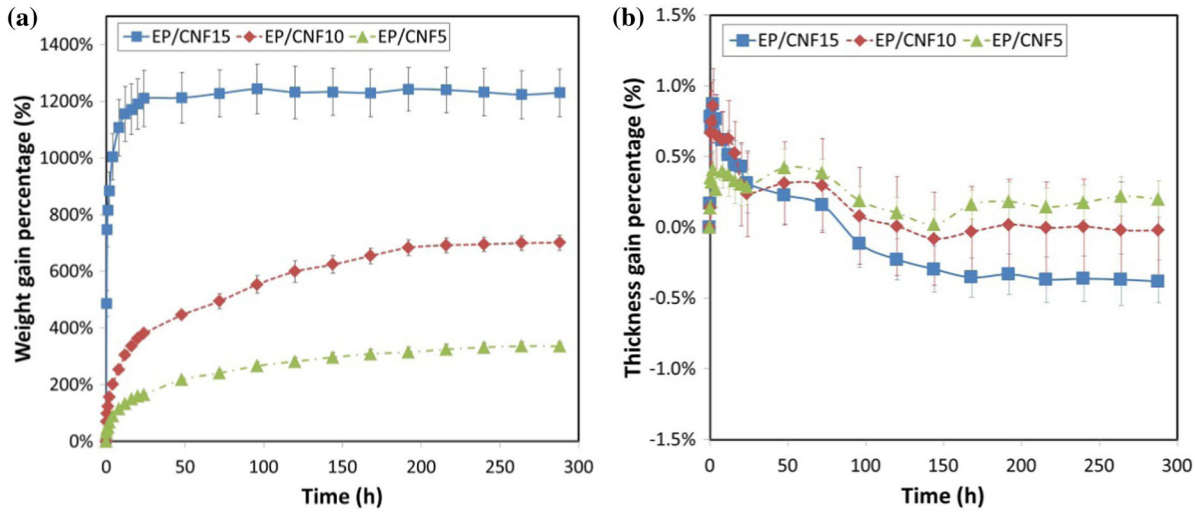

Fig. 6 **a** Weight gain percentage or water absorption of EP/CNF nanocomposites with different epoxy loadings; **b** thickness swelling gain of EP/CNF nanocomposites with different epoxy loadings

obtained for the samples with higher epoxy content, as expected. The absolute thickness swelling (TS) curves were also plotted in Fig. 6b, by the percentage thickness gain as a function of time. Results show thickness swelling of EP/CNF nanocomposite foams exhibited little change, within less than 1%, due to epoxy encapsulating the surfaces of hydrophilic CNFs which locked the skeleton structure without CNF dissolution. High epoxy loading contributed to stability in thickness swelling and epoxy, as a nanocomposite component, decreased water absorption and provided better dimensional stability of EP/CNF nanocomposite foam. Furthermore, water absorption rates of the EP/CNF nanocomposite foams were determined using Fick's law of diffusion model by water absorbed (MC) versus time$^{1/2}$ with a polynomial curve fitting at 2nd order (Wei et al. 2013). The diffusion coefficients D_f for EP/CNF15, EP/CNF10 and EP/CNF5 were 1.57 $\times$ 10^{-10} m^2/s, 0.32 $\times$ 10^{-10} m^2/s, and 0.28 $\times$ 10^{-10} m^2/s, respectively (Table 4). Results show increasing water absorption rates with decreased epoxy loading, and epoxy ratios in the nanocomposite were a major factor, causing differences in water absorption values. Samples exhibiting higher water absorption had higher diffusion coefficients. In the future, water absorption characteristics can be designed based on EP/CNF formulas for different applications.

Table 4 Water diffusion coefficient for each sample

Sample	Diffusion coefficient (10^{-10} m^2/s)
EP/CNF15	1.57
EP/CNF10	0.32
EP/CNF5	0.28

Crystalline structures

Wide angle XRD was used to determine the effect of CNF on the macro- and microstructure changes of EP/

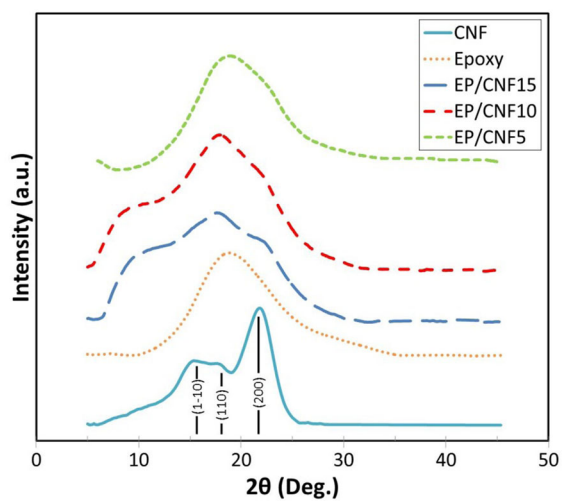

Fig. 7 XRD patterns of CNF, neat epoxy, and EP/CNF foam

CNF nanocomposite foams. Figure 7 shows the XRD patterns of CNF, epoxy and EP/CNF nanocomposites. The CNF displayed three main peaks at 15.3°, 17.6° and 21.8°, corresponding to diffractions of planes (1–10), (110) and (200), respectively (French 2014; Xu et al. 2013). For the neat epoxy sample, a wide diffraction from 10° to 35° was caused by scattering of cured epoxy molecules, indicating its amorphous nature (Wan et al. 2014). The result showed that the EP/CNF5 nanocomposite foam had similar diffraction patterns as the neat epoxy sample in Fig. 7. The three characteristic diffraction peaks of CNF had no apparent effect on EP/CNF 5 nanocomposite foam, demonstrating that low amounts of CNFs component in EP/CNF5 nanocomposite foam. EP/CNF15 and EP/CNF10 had higher amounts of CNFs than that of EP/CNF5, so the XRD pattern showed the some effect of CNFs on both samples. Furthermore, there was a new peak at 8.2° for EP/CNF15 and EP/CNF10 nanocomposite foams; it seems that some sort of longer-range organization was formed between CNFs and epoxy to cause the new peak, which might improve the mechanical performance. For EP/CNF5, due to the low amount of CNFs, no new peak was observed.

FTIR analysis

As shown in Fig. 8, FTIR spectra confirmed the chemical nature of CNFs, neat epoxy and EP/CNF foam. Accordingly, all samples presented two main absorbance regions in the range of 600–1800 cm^{-1} and 2600–3500 cm^{-1}. The FTIR spectra of all samples have shown a wide band in the region between 3200 and 3500 cm^{-1} that specifies the free O–H stretching vibration of the OH groups; however, the pure CNF sample has stronger intensity than that of neat epoxy and EP/CNF composite foams in this region. The spectrum of pure CNF samples showed C–H stretching vibration around 2900 cm^{-1}, which was different from the spectra of neat epoxy and EP/CNF composite foams with three peaks around 2962 cm^{-1} of C–H stretch of $–CH_3$ group, 2920 cm^{-1} of C–H stretch of $–CH_2$ group and 2870 $cm^{-1}$of C–H stretch of $–CH_3$ group. The band 1603 cm^{-1} was assigned to hydroxyl bending vibration of pure CNF sample, and the peaks at 1406, 1362, 1126, and 894 cm^{-1} were assumed the typical bonds of cellulose Iβ for pure CNF sample (Du et al. 2016). For neat epoxy and all EP/CNF composite, the spectra of FTIR had similar peaks: peak at 1606, 1579, 1504, and 1455 cm^{-1} corresponds to C–C stretching vibration in aromatic,

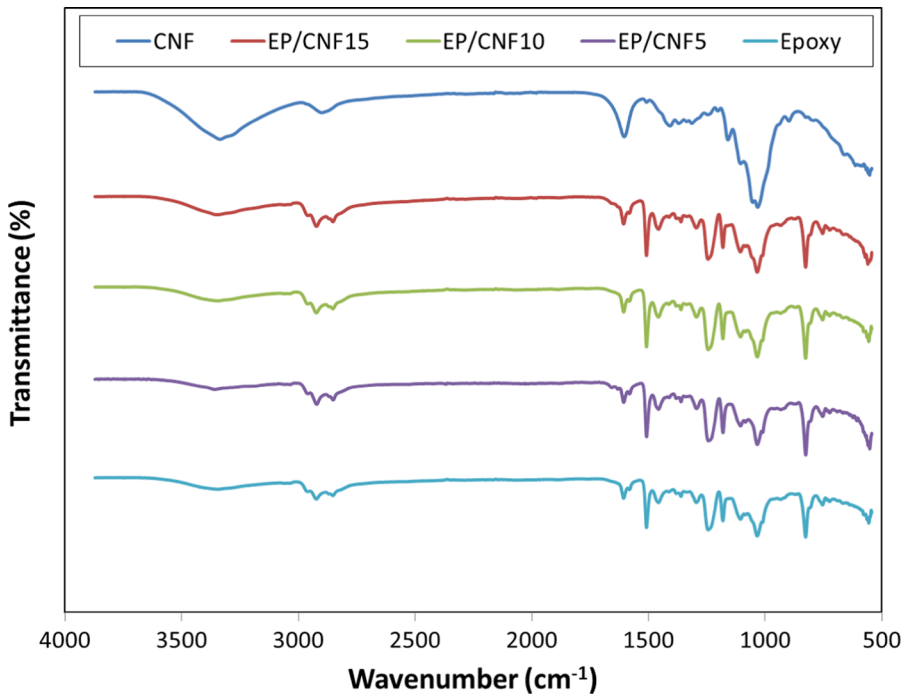

Fig. 8 FTIR spectra of CNFs, neat epoxy, and EP/CNF foam

peak at 1290 cm^{-1} corresponds to $–CH_2$ deformation, peak at 1240 cm^{-1} corresponds to aromatic C–O stretch, peak at 1180 cm^{-1} corresponds to aliphatic C–O stretch, peak at 1029 cm^{-1} corresponds to aromatic C–O stretch, peak at 1009, 930 and 866 cm^{-1} correspond to epoxide ring vibrations, and peak at 825 cm^{-1} corresponds to –CH out of plane deformation in aromatic (Maity et al. 2008). These FTIR result exhibited that the peaks of CNF in the spectra of these EP/CNF samples were overlapped by the peaks of epoxy, because the weight content of epoxy in these EP/CNF composite foams was significantly higher than the weight content of CNF component. Moreover, no apparent interaction between CNFs and epoxy can be found in Fig. 8.

Conclusions

In this paper, EP/CNF nanocomposite foam with a crosslinked structure was emulsified that showed alterable properties could be developed using a CNF suspension with epoxy resin. The EP/CNF emulsion was made by mechanical mixing and sonication, before freeze drying process to produce the EP/CNF nanocomposite foams. This process significantly improved their compressive performance for potential use in structural materials. The microstructures of EP/CNF composite foams with different EP/CNF weight ratio were investigated by scanning electron microscope. The surface morphology showed CNF crosslinked fibers were well encapsulated by epoxy resin through the emulsion process. The mechanical properties, water resistance, and thermal stability of EP/CNF composites foams were measured using a compression test, water absorption test, and thermogravimetric analysis. The EP/CNF ratio was shown to have a significant effect on the compressive properties and water resistance. Samples with higher epoxy levels exhibited many micro-ribs between the CNF walls. After epoxy encapsulation of the CNF surfaces, the foams provided better compressive properties, better water resistance, and better thermal stability. The glass transition temperature (T_g) was determined by differential scanning calorimetry. T_g of the nanocomposite foams was influenced by the EP/CNF composition. Therefore, the properties of EP/CNF nanocomposite foams can be modified via changing the weight ratio between epoxy resin and CNF suspension. Compared with resin/solvent infusion process, this method is more cost efficient and simple to fabricate CNF composite foam.

References

Ahmadzadeh S, Keramat J, Nasirpour A, Hamdami N, Behzad T, Aranda L, Vilasi M, Desobry S (2016) Structural and mechanical properties of clay nanocomposite foams based on cellulose for the food-packaging industry. J Appl Polym Sci 133:510–520

ASTM D570 (1998) Standard test method for water absorption of plastics. American Society for Testing and Materials, New York

ASTM D695 (2010) Standard test method for compressive properties of rigid plastics. ASTM International, West Conshohocken

Bledzki AK, Gassan J (1999) Composites reinforced with cellulose based fibres. Prog Polym Sci 24:221–274

Chen B, Zheng Q, Zhu J, Li J, Cai Z, Chen L, Gong S (2016) Mechanically strong fully biobased anisotropic cellulose aerogels. RSC Adv 6:96518–96526

Du H, Liu C, Mu X, Gong W, Lv D, Hong Y, Si C, Li B (2016) Preparation and characterization of thermally stable cellulose nanocrystals via a sustainable approach of $FeCl_3$-catalyzed formic acid hydrolysis. Cellulose 23:2389–2407

Fowler PA, Hughes JM, Elias RM (2006) Biocomposites: technology, environmental credentials and market forces. J Sci Food Agric 86:1781–1789

French AD (2014) Idealized powder diffraction patterns for cellulose polymorphs. Cellulose 21:885–896

Han J, Yue Y, Wu Q, Huang C, Pan H, Zhan X, Mei C, Xu X (2017) Effects of nanocellulose on the structure and properties of poly(vinyl alcohol)-borax hybrid foams. Cellulose 24:4433–4448

Hodgkin JH, Simon GP, Varley RJ (1998) Thermoplastic toughening of epoxy resins: a critical review. Polym Adv Technol 9:3–10

Jeronimidis G (1979) Wood, one of nature's challenging composites. Symp Soc Exp Biol 34:169–182

Khalil HPSA, Bhat AH, Yusra AFI (2012) Green composites from sustainable cellulose nanofibrils: a review. Carbohydr Polym 87:963–979

Kord B (2013) Effect of nanoclay on thickness swelling behavior in the extrusion foaming of wood flour/polyethylene composites. J Thermoplast Compos 26:1303–1316

Lee S-Y, Chun S-J, Kang I-A, Park J-Y (2009) Preparation of cellulose nanofibrils by high-pressure homogenizer and cellulose-based composite films. J Ind Eng Chem 15:50–55

Leng W, Li J, Cai Z (2017) Synthesis and characterization of cellulose nanofibril-reinforced polyurethane foam. Polymers 9:597

Li J, Hunt JF, Gong S, Cai Z (2014a) High strength wood-based sandwich panels reinforced with fiberglass and foam. BioResources 9:1898–1913

Li Z, Yao C, Wang F, Cai Z, Wang X (2014b) Cellulose nanofiber-templated three-dimension TiO_2 hierarchical nanowire network for photoelectrochemical photoanode. Nanotechnology 25:504005

Li J, Hunt JF, Gong S, Cai Z (2017a) Low-velocity impact and compressive behavior for shifted-tri-axial composite panels. J Sandw Struct Mater. https://doi.org/10.1177/1099636217697498

Li J, Hunt JF, Gong S, Cai Z (2017b) Quasi-static compression and low-velocity impact behavior of tri-axial bio-composite structural panels using a spherical head. Materials 10:185

Li J, Wei L, Leng W, Hunt JF, Cai Z (2018) Fabrication and characterization of cellulose nanofibrils/epoxy nanocomposite foam. J Mater Sci 53:4949–4960

Maity P, Kasisomayajula SV, Parameswaran V, Basu S, Gupta N (2008) Improvement in surface degradation properties of polymer composites due to pre-processed nanometric alumina fillers. IEEE Trans Dielectr Electr Insul 15:63

Saito T, Hirota M, Tamura N, Kimura S, Fukuzumi H, Heux L, Isogai A (2009) Individualization of nano-sized plant cellulose fibrils by direct surface carboxylation using TEMPO catalyst under neutral conditions. Biomacromolecules 10:1992–1996

Soni B, Mahmoud B (2015) Chemical isolation and characterization of different cellulose nanofibers from cotton stalks. Carbohydr Polym 134:581–589

Wan YJ, Gong LX, Tang LC, Wu LB, Jiang JX (2014) Mechanical properties of epoxy composites filled with silane-functionalized graphene oxide. Compos A Appl S 64:79–89

Wei L, McDonald AG, Freitag C, Morrell JJ (2013) Effects of wood fiber esterification on properties, weatherability and biodurability of wood plastic composites. Polym Degrad Stab 98:1348–1361

Xu X, Liu F, Jiang L, Zhu J, Haagenson D, Wiesenborn DP (2013) Cellulose nanocrystals vs. cellulose nanofibrils: a comparative study on their microstructures and effects as polymer reinforcing agents. ACS Appl Mater Interfaces 5:2999–3009

Zhang J, Luo N, Zhang X, Xu L, Wu J, Yu J, He J, Zhang J (2016) All-cellulose nanocomposites reinforced with in situ retained cellulose nanocrystals during selective dissolution of cellulose in an ionic liquid. ACS Sustain Chem Eng 4:4417–4423

Zheng Q, Cai Z, Gong S (2014) Green synthesis of polyvinyl alcohol (PVA)–cellulose nanofibril (CNF) hybrid aerogels and their use as superabsorbents. J Mater Chem A 2:3110–3118

Zheng Q, Cai Z, Ma Z, Gong S (2015) Cellulose nanofibril/reduced graphene oxide/carbon nanotube hybrid aerogels for highly flexible and all-solid-state supercapacitors. ACS Appl Mater Interfaces 7:3263–3271